electronics

MDPI

Article

Design of a Tunnel Anchor Monitoring System Based on Long Short-Term Memory–Autoregressive Integrated Moving Average Prediction

Junyan Qi [1], Yuhao Che [1,*], Lei Wang [2] and Ruifu Yuan [3]

[1] School of Software, Henan Polytechnic University, Jiaozuo 454000, China; qjywl@hpu.edu.cn
[2] School of Computer Science and Technology, Henan Polytechnic University, Jiaozuo 454000, China; wlqjy@hpu.edu.cn
[3] School of Surveying and Land Information Engineering, Henan Polytechnic University, Jiaozuo 454000, China; yrf@hpu.edu.cn
* Correspondence: 212209010008@home.hpu.edu.cn

Abstract: Considering the shortcomings of the current monitoring system for tunnel anchor support systems, a tunnel anchor monitoring system based on LSTM-ARIMA prediction is proposed in this paper to prevent the deformation and collapse accidents that may occur in the underground mine tunnels during the backfilling process, which combines the Internet of Things and a neural network deep learning algorithm to achieve the real-time monitoring and prediction of the tunnel anchor pressure. To improve the prediction accuracy, a time series analysis algorithm is used in the prediction model of this system. In particular, an LSTM-ARIMA model is constructed to predict the tunnel anchor pressure by combining the Long Short-Term Memory (LSTM) model and the Autoregressive Integrated Moving Average (ARIMA) model. And a dynamic weighted combination method is designed based on model prediction confidence to acquire the optimal weight coefficients. This combined model enables the monitoring system to predict the anchor pressure more accurately, thereby preventing possible tunnel deformation and collapse accidents in advance. Finally, the overall system is verified using the anchor pressure dataset obtained from the 21,404 section of the Hulusu Coal Mine transportation tunnel in real-world engineering, whose results show that the pressure value predicted using the combined model is basically the same as the actual value on site, and the system has high real-time performance and stability, proving the effectiveness and reliability of the system.

Keywords: anchor monitoring; system development; LSTM-ARIM; anchor pressure prediction

Citation: Qi, J.; Che, Y.; Wang, L.; Yuan, R. Design of a Tunnel Anchor Monitoring System Based on Long Short-Term Memory–Autoregressive Integrated Moving Average Prediction. *Electronics* **2024**, *13*, 2840. https://doi.org/10.3390/electronics13142840

Academic Editor: Ahmed Abu-Siada

Received: 23 June 2024
Revised: 12 July 2024
Accepted: 15 July 2024
Published: 19 July 2024

1. Introduction

The coal resource is an important core resource for promoting social progress and is a driving force for rapid economic development in the early stages [1]. In order to meet the demand for coal energy, the demand for coal is constantly increasing, and with it come the safety issues brought about by coal mining. In particular, during the mining process of coal mine working faces, the deformation of the rock mass around the tunnel and the change in stress distribution may lead to tunnel deformation, landslides, roof falls, and other disasters [2–4].

The tunnel anchor is a type of support structure widely used in coal mine tunnels. Currently, almost all coal mine tunnels in developed countries use anchor support technology. In China, anchor support accounts for over 75% of the total tunnel support [5,6]. The stress state of the tunnel anchor is a key indicator for measuring tunnel stability and is of great significance for preventing tunnel accidents, ensuring personnel safety, and guiding engineering construction [7]. Therefore, the real-time monitoring and prediction of the stress state of tunnel anchors is an urgent and necessary task. At present, there are many studies using different methods to monitor the pressure of tunnel anchors. Some

researchers [8] install a non-destructive anchor (cable) dynamometer between the anchor tray and the surrounding rock to measure the actual force of the anchor and its change over time. Some researchers [9] propose a method for monitoring the stress of tunnel anchor rods based on grating sensors, which can achieve the real-time monitoring of pressure, displacement, the stress of the tunnel surrounding rock, and the stress of the anchor rods. In addition, a mining fiber grating anchor rod sensor technology for monitoring the stress of the anchor rod body is proposed in [10], which analyzes the stress change law of the rod body and predicts and warns of the fracture of the rod body. In [11], the real-time safety status of the roadway anchor is analyzed by comparing the real-time status of the Fiber Bragg Grating (FBG) anchor sensor with the axial force variation of the anchor in service on the mining roadway. Some researchers [12] independently develop an anchor FBG stress sensor based on FBG sensor technology, revealing the safety status and evolution law of the anchor in service on the mining roadway. In terms of anchor pressure prediction, the anchor support state is predicted based on multi-parameter input and output Gaussian process regression in [13]. Some researchers [14] established two coupling models and derived the constitutive equations of the models and the change formula of effective pre-stress, verifying the rationality and accuracy of the segmented prediction model. However, there are still some problems in the monitoring and prediction of anchor pressure in tunnels. In terms of monitoring, traditional monitoring methods mainly rely on manual or wired transmission, which is inefficient, costly, and susceptible to various interferences. In addition, existing monitoring methods mainly focus on hardware monitoring and lack effective integration with real-time systems. In terms of prediction, many current monitoring systems do not have the ability to predict the trend in anchor pressure changes, and most of the existing prediction methods use mathematical modeling methods for prediction, which are not combined with artificial intelligence. The prediction effect is not ideal, and the accuracy needs to be improved.

In order to make up for the shortcomings of the existing tunnel anchor monitoring system and prediction, a tunnel anchor monitoring system based on LSTM-ARIMA prediction is designed and developed in this paper. The system formats and stores the collected data through a set software interface to achieve the real-time monitoring of the anchor stress condition. In addition, the LSTM-ARIMA combined algorithm is used in this system to predict the trend in anchor pressure changes.

2. System Design

2.1. System Function Design

The main functions of the system can be divided into four modules, as follows: tunnel management, equipment management, monitoring center, and prediction center.

(1) Tunnel management module: this module can manage the relevant information about underground tunnels, including setting the information about allocated tunnels and the number of anchors installed in the tunnels, as well as setting the current tunnel theme to ensure that the data between sensors in different tunnels do not conflict with each other.

(2) Equipment management module: This module includes equipment mapping and an equipment data list. Equipment mapping can set the correspondence between the actual ID of the downhole sensor and its position in the tunnel. The overall process is shown in Figure 1. The equipment data list is used to display the data of all sensors and can be filtered, viewed, queried, etc. At the same time, historical pressure data can be exported in different formats at different times. Its interface is shown in Figure 2.

(3) Monitoring center module: users can view the historical monitoring data and status information of each device in real time through bar charts, line charts, and pie charts.

(4) Prediction center: as shown in Figure 3, this module analyzes and models historical monitoring data to predict the future stress state of the equipment.

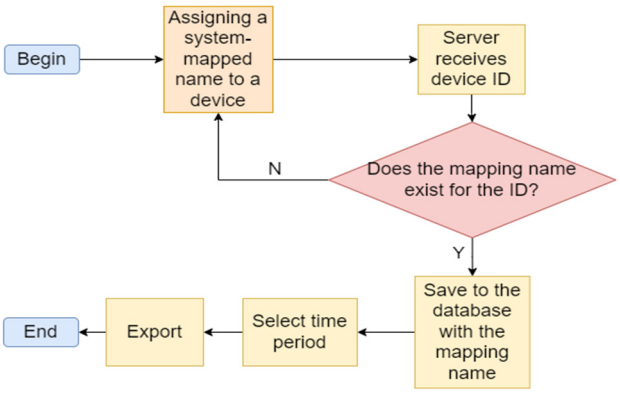

Figure 1. Device management module flowchart.

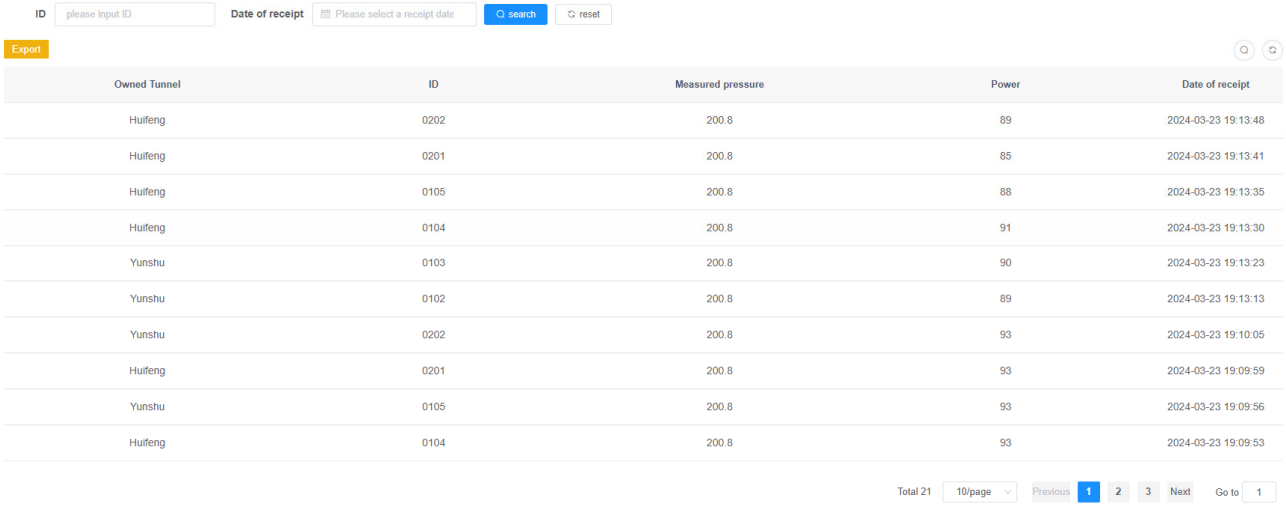

Figure 2. Equipment monitoring data list interface.

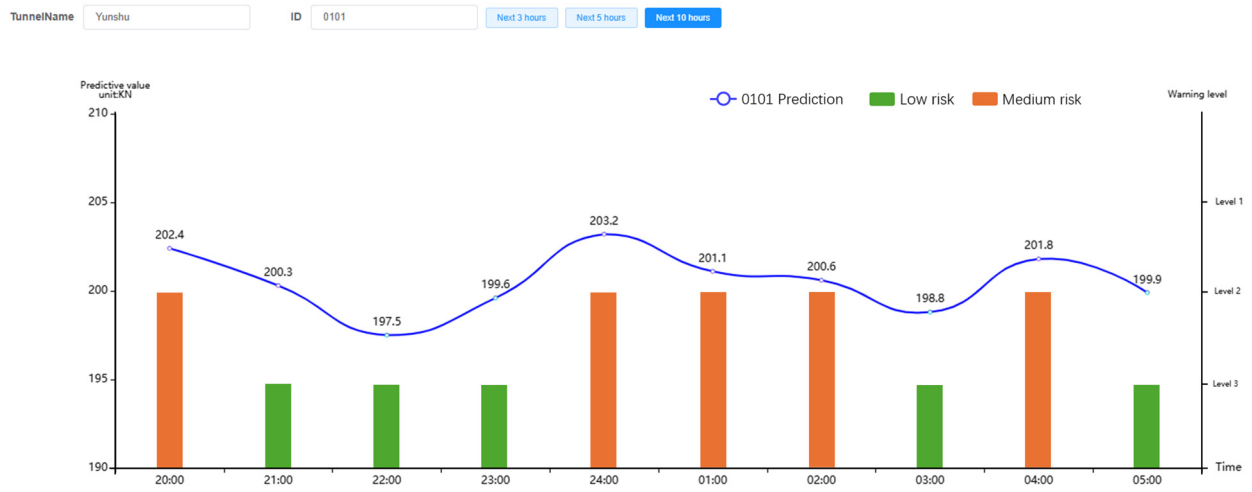

Figure 3. Anchor pressure prediction interface.

2.2. System Architecture Design

The overall system architecture adopts a layered design, which includes the data collection layer, the data transmission layer, the data storage and logic processing layer, and the front-end application display layer from bottom to top, as shown in Figure 4.

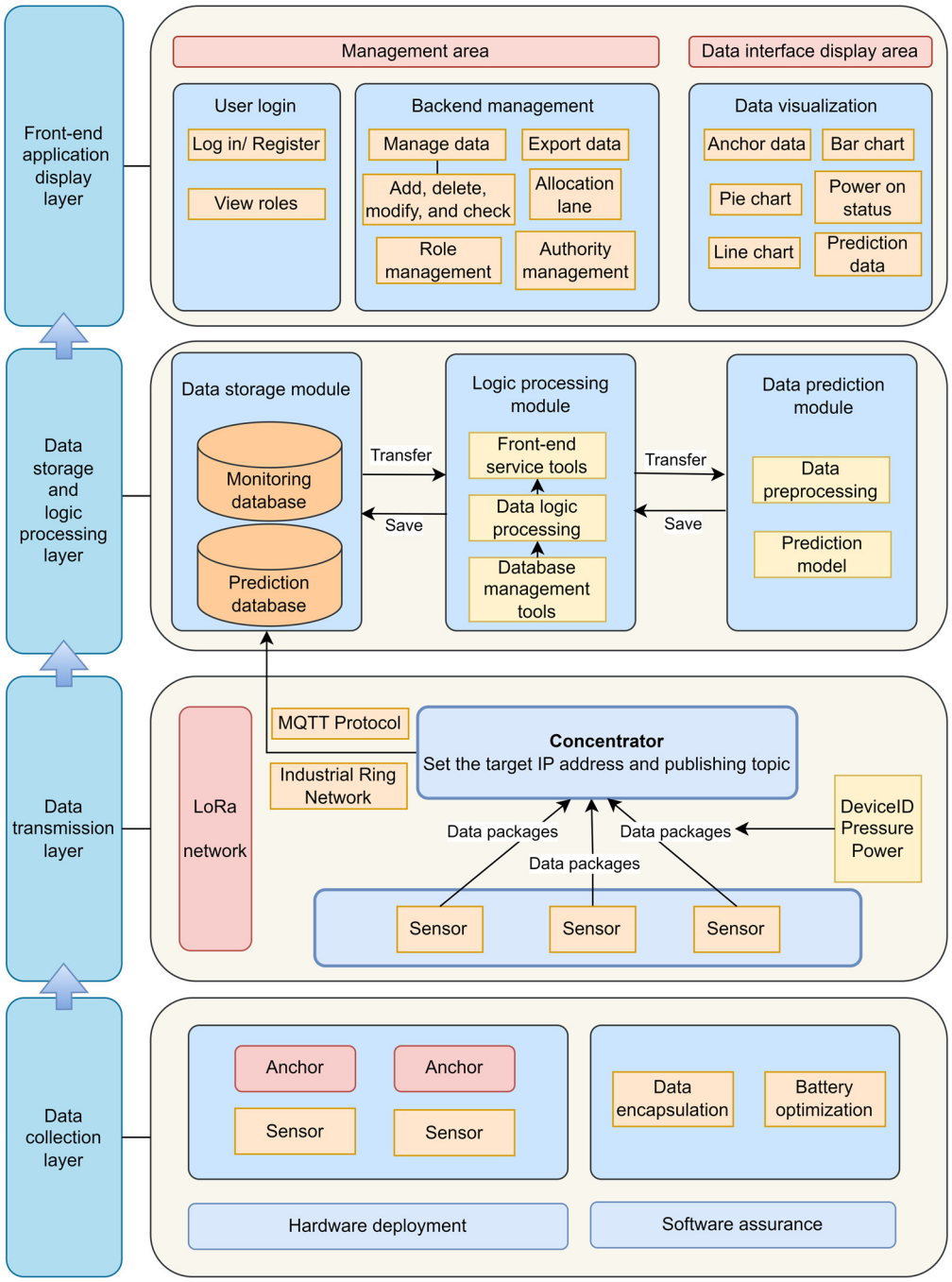

Figure 4. Overall architecture of the system.

(1) Data acquisition layer: This layer is the foundation of the entire system and is the source of data acquisition. This layer integrates sensors, concentrators, and long-distance wireless communication networks to form a complete data acquisition and transmission system. The on-site installation method is shown in Figure 5.

(2) Data transmission layer: The data transmission layer plays a key role in connecting the upper and lower layers. The concentrator can effectively and accurately transmit data in a timely manner to the upper layer through the industrial ring network. The industrial ring network can ensure continuous data transmission and the stable operation of the system even in the event of equipment failure or network interruption. This design not only improves the real-time accuracy of data, but also enhances the stability and reliability of the system.

(3) Data storage and logic processing layer: This layer is the core component of the system and mainly includes a data storage module, a logic processing module, and a data prediction module. To be specific, the data storage module is responsible for storing data. The logic processing module is responsible for performing various complex data processing and analysis tasks. The data prediction module performs predictive analysis on real-time data and sends the prediction results to the data storage module for storage.

(4) Application display layer: this layer is used for the visual display of real-time monitoring data and prediction data, as shown in Figure 6.

Figure 5. On-site installation of concentrators and sensors.

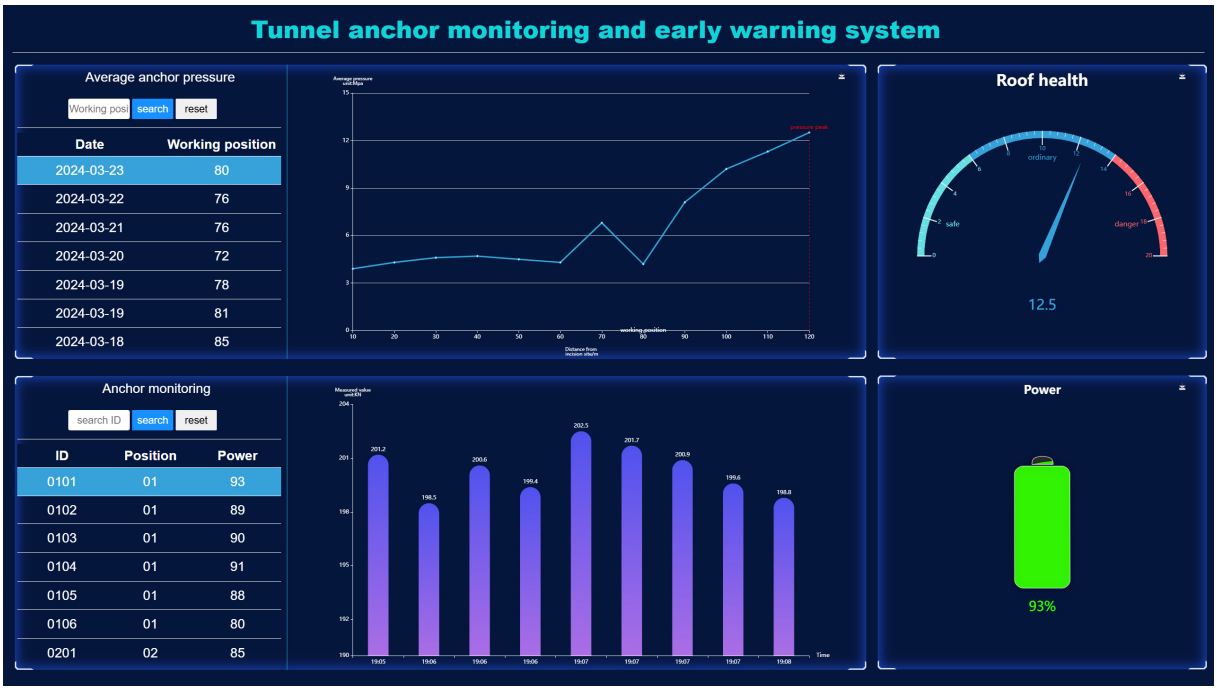

Figure 6. Visual monitoring screen.

3. Data Collection and Transmission

3.1. Concentrator Design

The concentrator mainly includes modules such as a control panel, a display screen, a switch, and a Long-Range Radio (LoRa) gateway. Figure 7 shows the overall design framework of the concentrator. The WAN port of the LoRa gateway is connected to the switch through a network cable. The switch is connected to the lane base station through a network cable or optical fiber and transmits data to the system server through an industrial ring network. In order to enhance the transmission distance of the LoRa wireless network,

the concentrator is equipped with a LoRa directional antenna with a frequency band of 433 MHz and a gain of 6 dBi (Figure 8). The directional antenna sets a specific frequency transmission rate. After testing, the maximum transmission distance of LoRa can reach 1 km under the same network.

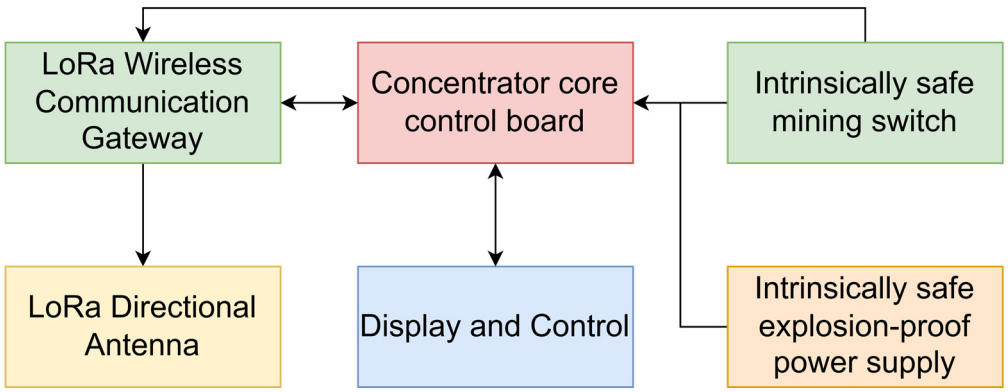

Figure 7. Concentrator overall design framework.

Figure 8. Concentrator gain antenna.

3.2. Sensor Installation and Collection

Figure 9 shows the sensor installation and data collection method. The sensor is installed between the anchor nut and the tray, as shown in Figure 9a. The sensor converts the pressure received into an electrical signal and transmits it to the data collector through the data line. Figure 9b shows the installation method of the sensor on a section of the tunnel. A total of seven sensors are installed on a section.

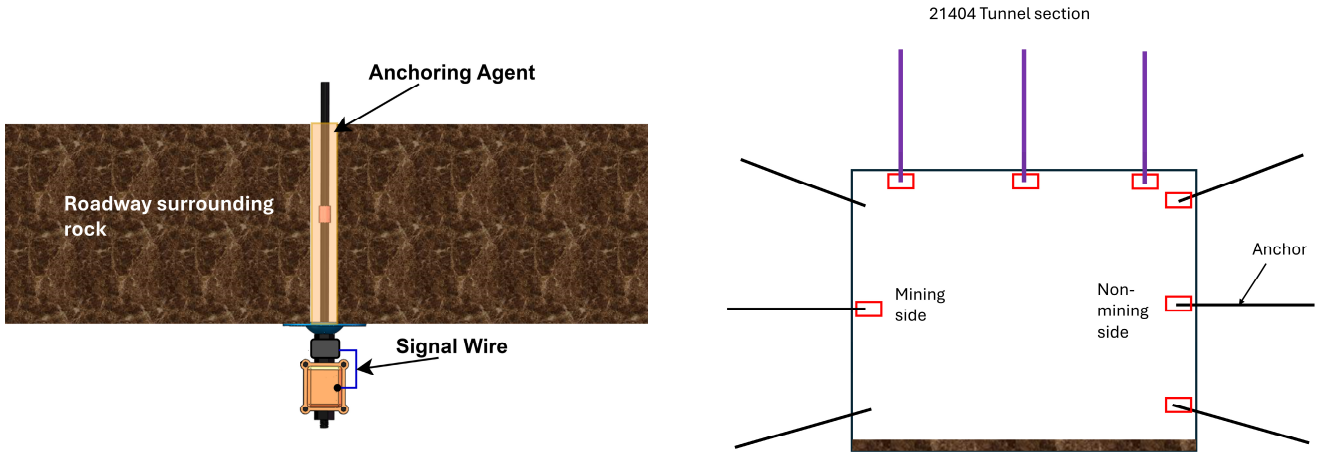

(**a**) Sensor installation method (**b**) Tunnel cross-section sensor installation diagram

Figure 9. Sensor installation and collection.

In the tunnel monitored in the actual project, the installation method is shown in Figure 10. A row of sensors is installed in every six sections, and the distance between two monitoring sections is about 7.2 m.

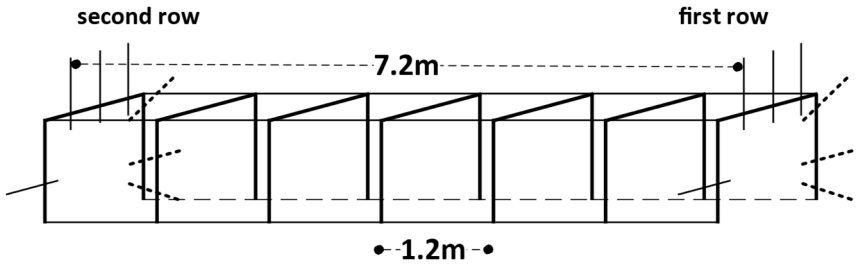

Figure 10. Schematic diagram of actual tunnel sensor installation.

3.3. Data Transmission

In the 500 m installation range of the tunnel, the concentrator and antenna are installed in the middle of the range to maximize the data reception of each row of collectors, as shown in Figure 11. The overall transmission mode of the tunnel sensor is shown in Figure 12. Each collector sends data to the concentrator through the LoRa network, and the concentrator sends data to the cloud platform server through the industrial ring network using the Message Queuing Telemetry Transport (MQTT) protocol. This design framework and layout ensure that the stress monitoring data in the coal mine tunnel can be stably and accurately transmitted to the ground system server, providing reliable data support for coal mine safety production.

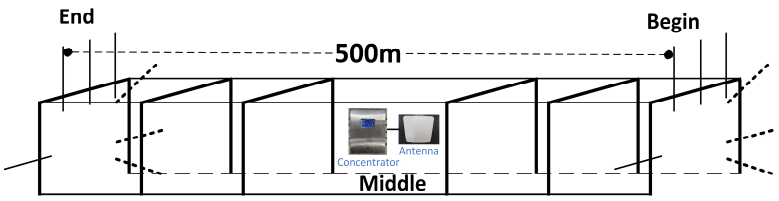

Figure 11. Concentrator installation diagram.

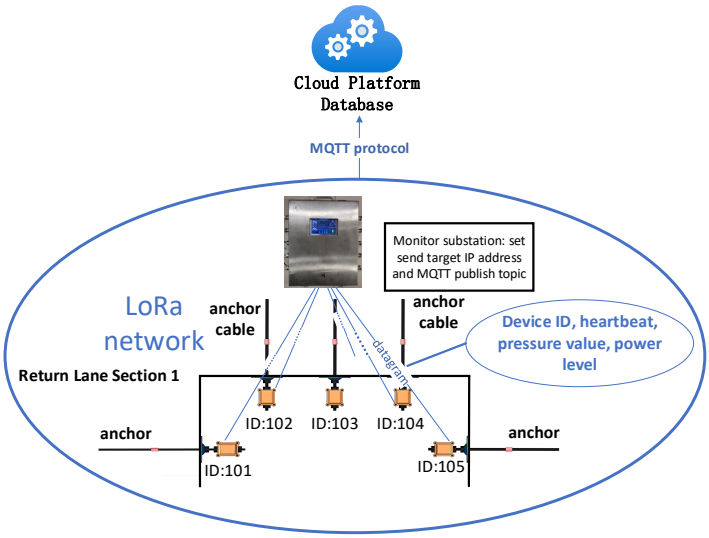

Figure 12. Sensor data transmission method.

4. Prediction Model

4.1. Long Short-Term Memory Network (LSTM)

The LSTM neural network is an improved architecture of the recurrent neural network (RNN). RNNs are a type of neural network model with feedback connections. They can combine previous time series information to generate output information for the next moment. They are a neural network specifically used to process sequential data [15]. Its structure is shown in Figure 13.

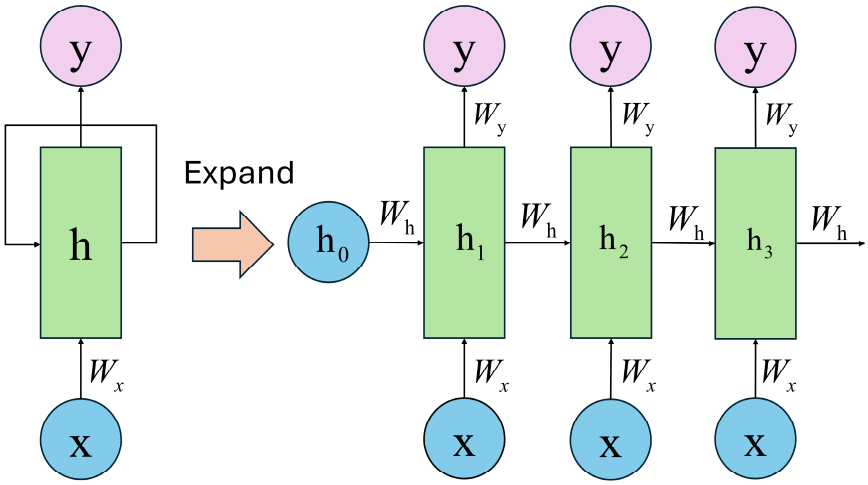

Figure 13. RNN structure and its expansion.

The RNN model has advantages in processing sequence data and time correlation, but it has short-term memory problems and gradient vanishing and exploding problems. To solve the above problems, Schmidhuber et al. first proposed LSTM in 1997 [16]. LSTM introduces a gating mechanism, including a forget gate, an input gate, and an output gate [17]. The gate unit controls the retention and forgetting of information, which can effectively solve the long-term dependence of information and avoid gradients vanishing or exploding [18]. The LSTM network is composed of multiple LSTM cells. Figure 14a shows the structure of the LSTM cell, and Figure 14b shows how to construct a complete LSTM network through the connection between multiple LSTM cells.

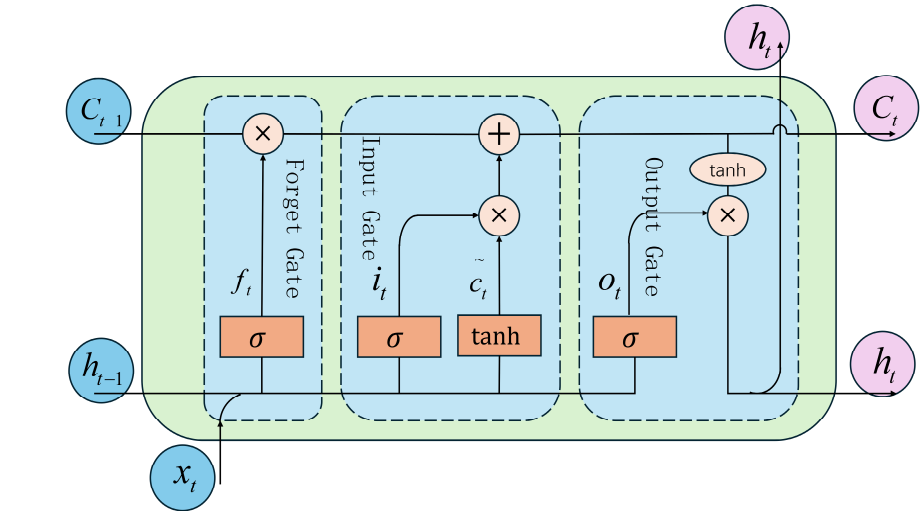

(**a**) LSTM cell structure

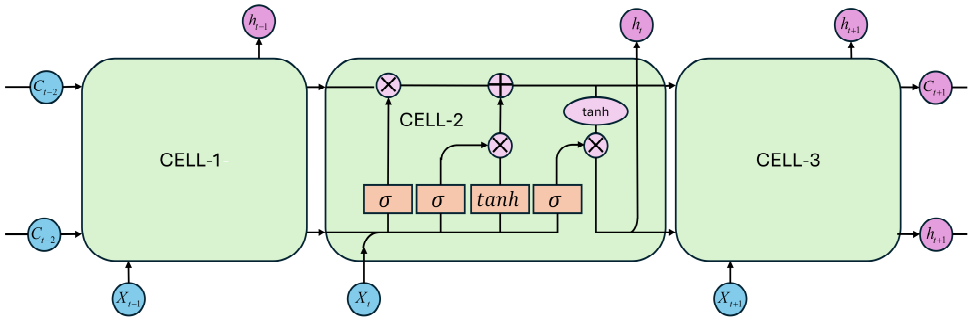

(**b**) LSTM neural network expansion

Figure 14. LSTM cell structure diagram and neural network unfolding diagram.

In addition, in order to increase the ability of LSTM cells to capture information in the long term, C_t is added to the cell as a new internal state. The calculation formula for the forget gate is as follows:

$$f_t = \sigma(W_f \cdot x_t + W_f \cdot h_{t-1} + b_f) \tag{1}$$

$$\sigma(x) = \frac{1}{1 + e^{-x}} \tag{2}$$

Among them, the role of the sigmoid activation function, $\sigma(x)$, is to filter information so that LSTM cells can maintain a long-term memory of information. The calculation formula for the input gate is as follows:

$$i_t = \sigma(W_i \cdot x_t + W_i \cdot h_{t-1} + b_i) \tag{3}$$

$$\widetilde{c}_t = tanh(W_c \cdot x_t + W_c \cdot h_{t-1} + b_c) \tag{4}$$

$$tanh(x) = 2\sigma(2x) - 1 \tag{5}$$

Among them, the sigmoid activation function is used to update the cell state, and its calculation process is as follows:

$$C_t = f_t \cdot C_{t-1} + i_t \cdot \widetilde{c}_t \tag{6}$$

$$\sigma_t = \sigma(W_o \cdot x_t + W_o \cdot h_{t-1} + b_o) \tag{7}$$

$$h_t = o_t \cdot tanh(C_t) \tag{8}$$

Among them, h_t is the output of the LSTM cell, which is calculated using the sigmoid activation function and the *tanh* activation function.

4.2. Autoregressive Moving Average (ARIMA)

The ARIMA (Autoregressive Integrated Moving Average) model is one of the more commonly used time series prediction methods [19]. The model can handle linear trends and seasonal changes well. At present, the prediction and comprehensive analysis model combining ARIMA and other methods with neural networks has achieved good results in the prediction work in the field of mining engineering [20]. The ARIMA (p, d, q) model can perform d-order difference transport on non-stationary time series. The goal of the difference is to transform the non-stationary series into a stationary series [21,22]. The mathematical expression of the ARMA model is:

$$X_t = C + w_t + \sum_{i=1}^{p} q_i x_{t-i} - \sum_{i=1}^{q} B_i q_{t-q} \tag{9}$$

Among them, p represents the autoregressive part (autoregressive). The specific mathematical form is as follows:

$$Y_t = c + \varphi_1 Y_{t-1} + \varphi_2 Y_{t-2} + \ldots + \varphi_p Y_{t-p} + \xi_t \tag{10}$$

Among them, Y_t is the time series after stabilization, $\epsilon_{t-1}, \epsilon_{t-2}, \ldots, \epsilon_{t-q}$ is the model parameter, c is a constant, and ξ_t is white noise. The moving average model establishes a relationship between the current value and the past white noise. The specific mathematical form is as follows:

$$Y_t = \mu + \epsilon_t + \theta_1 \epsilon_{t-1} + \theta_2 \epsilon_{t-2} + \cdots + \theta_q \epsilon_{t-q} \tag{11}$$

Among them, Y_t is the time series after stabilization, $\theta_1, \theta_2, \ldots, \theta_q$ is the model parameter, ϵ_t is the white noise of the current period, and $\epsilon_{t-1}, \epsilon_{t-2}, \ldots, \epsilon_{t-q}$ is the white noise of the past. The order q of this equation determines the amount of white noise in the model.

The selection of p, d, and q values in the ARIMA model is mainly based on the Akaike Information Criterion (AIC) [23]. It is generally believed that the smaller the AIC value, the better the prediction effect of the model will be.

4.3. LSTM–ARIMA Combined Forecasting Model

In terms of processing time series data, LSTM can learn the patterns and trends in data by training historical anchor pressure data, handling long-term dependencies and nonlinear data, and predicting the results of future anchor pressure, which is more advantageous than ARIMA. The pressure data collected from the same anchor for 10 days are shown in Figure 15. It can be seen that the anchor pressure also shows a seasonal trend, but the LSTM model does not have a good advantage in processing data with seasonal trends. In contrast, the ARIMA model is a time series prediction model based on linear regression, which can handle linear trends and seasonal changes well. Therefore, the ARIMA model can effectively make up for the shortcomings of the LSTM model in processing seasonal trend data. In order to achieve the goal of accurately predicting anchor pressure data, a combined prediction method of LSTM and ARIMA is presented in this paper, which can simultaneously utilize the advantages of the two models. No matter what trend or pattern the data presents, the combined model can capture the law of anchor pressure data and improve the accuracy of the prediction. In addition, the combined model can reduce the risk of overfitting a single model, thereby improving the prediction ability of the overall model on unknown data. Therefore, combining these two models for prediction can make full use of their respective advantages and improve the stability of the model. At the same time, in terms of combination, a dynamic weighting method based on confidence is adopted to further improve the accuracy of the combined model prediction. The following is the main process of the combination:

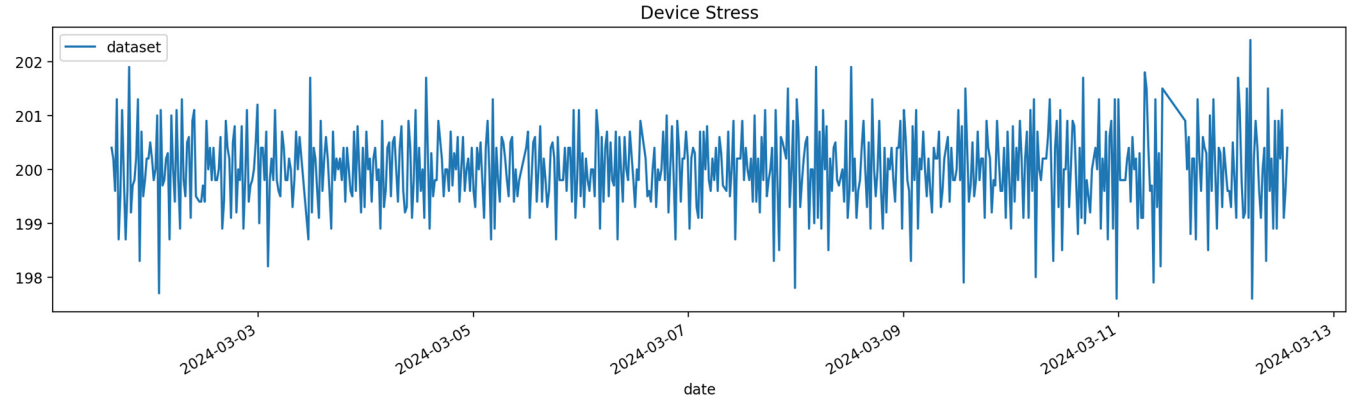

Figure 15. Anchor pressure data.

First, the LSTM and ARIMA models are used to predict the time series anchor pressure data, respectively, to obtain their respective prediction results. In order to measure the reliability of the prediction results of each model, its prediction error is calculated, and the inverse of the error is used as the confidence to evaluate the model.

Root Mean Square Error (RMSE) is a commonly used error measurement method that can effectively measure the difference between the predicted value and the actual observed value. RMSE gives a greater penalty for large errors, and it is particularly suitable for situations where large prediction errors are desired to be avoided. Therefore, RMSE is used to measure the difference between each predicted value and the actual observed value of the LSTM and ARIMA models. A smaller RMSE value means that the model's prediction at that point in time is more accurate and therefore has a higher confidence level. Its calculation formula is:

$$RMSE = \sqrt{\frac{1}{n}\sum_{i=1}^{n}(y_i - \hat{y}_i)^2} \tag{12}$$

Among them, y_i is the true value, and $\hat{y}_i$ is the predicted value. According to RMASE, the LSTM model error, e_{LSTM}, and ARIMA error, e_{LSTM}, can be calculated. Thus, the confidence of LSTM and ARIMA can be further obtained, and the calculation formula is:

$$conf_{LSTM} = 1/e_{LSTM} \tag{13}$$

$$conf_{ARIMA} = 1/e_{ARIMA} \tag{14}$$

Among them, conf is the confidence of the model. According to the model confidence, the weight of each model can be obtained. The calculation formula is:

$$w_{LSTM} = \frac{conf_{LSTM}}{conf_{LSTM} + conf_{ARIMA}} \tag{15}$$

$$w_{ARIMA} = \frac{conf_{ARIMA}}{conf_{LSTM} + conf_{ARIMA}} \tag{16}$$

Among them, w_{LSTM} and w_{ARIMA} are the weights of LSTM and ARIMA. After obtaining the weights, the prediction results of the LSTM and the ARIMA model are weighted to obtain the final prediction results. The calculation formula is:

$$\hat{y}_{final} = w_{LSTM} \cdot \hat{y}_{LSTM} + w_{ARIMA} \cdot \hat{y}_{ARIMA} \tag{17}$$

Among them, $\hat{y}_{LSTM}$ and $\hat{y}_{ARIMA}$ are the prediction results of the LSTM and the ARIMA models, respectively, and $\hat{y}_{final}$ is the prediction result of the combined model.

In the combined model, the model will calculate the error of each model based on the first 100 predicted values and true values to dynamically adjust the weights. This dynamic weight adjustment strategy can adaptively allocate weights based on confidence, so the

model with better performance occupies a larger proportion in the combination. In this way, the advantages of the LSTM and ARIMA models can be better utilized to improve the accuracy of predictions.

5. System Function Verification

5.1. Real-Time Analysis

First, the delay of data acquisition and transmission is analyzed in detail. The location of data acquisition is considered and the timestamps of data acquisition and transmission in the actual project are recorded, these are compared with the time when the actual system receives the data to evaluate the system's performance in terms of real-time performance. In addition, the location of data acquisition also needs to be considered. The transmission distance between different locations will affect the real-time performance of the system. When the transmission distance is longer, the data transmission time usually increases, resulting in an increased delay. For different data acquisition locations, the test results are shown in Table 1.

Table 1. Real-time performance test results of monitoring system.

Testing Frequency	Transmission Distance (m)	Sending Timestamp	Receive Timestamp	Delay (s)	Theoretical Delay (s)
1	1000	18:23:36:346	18:23:36:867	0.521	0.428
2	1000	18:23:46:353	18:23:46:846	0.493	0.428
3	1000	18:23:55:867	18:23:56:356	0.489	0.428
4	1200	18:29:09:427	18:29:10:065	0.638	0.594
5	1200	16:29:10:112	16:29:10:804	0.692	0.594
6	1200	16:29:19:894	16:29:20:565	0.671	0.594
7	1500	16:37:26:395	16:37:27:279	0.884	0.813
8	1500	16:37:36:218	16:37:37:103	0.865	0.813
9	1500	16:37:47:102	16:37:47:993	0.891	0.813
10	2000	16:57:38:541	16:57:40:019	1.478	1.324
11	2000	16:57:49:086	16:57:50:592	1.506	1.324
12	2000	16:58:01:139	16:58:02:631	1.492	1.324

The delay is calculated as follows:

$$T_{total} = T_{trans} + T_{prop} \tag{18}$$

Among them, T_{trans} is the transmission delay, which is calculated as L/B. L is the size of the MQTT protocol data packet (including the request header, data, topic, etc.), and B is the link bandwidth. T_{prop} is the propagation delay, which is calculated as d/s; d is the transmission distance; and s is the signal propagation speed.

In actual tunnels, the distance between the data collector and the concentrator is usually within 500 m, and the distance between the concentrator and the server is about 1000 m. As can be seen from Table 1, when the transmission distance is less than 1500 m, the average delay is 0.88 s, the error is controlled within 1 s, and the data collector sends data every 30 min. Therefore, a delay of 1 s can meet the real-time requirements, which verifies the real-time performance of the monitoring system in the monitoring of bolt support in coal mine tunnels.

5.2. Reliability Analysis

This study uses the method of simulating network interruptions to verify the reliability of the system. The system's ability to respond to a data transmission interruption is evaluated by artificially interrupting the connection during data transmission to simulate a network failure. The simulation was interrupted 50 times, and the results showed that the network could be reconnected normally and data transmission could be maintained stably after the network was restored. As shown in Figure 16, the system is able to quickly

detect the transmission interruption and re-establish communication after the connection is restored to ensure data integrity and continuity. This verifies that the system can effectively respond and maintain reliable monitoring when faced with data transmission interruptions.

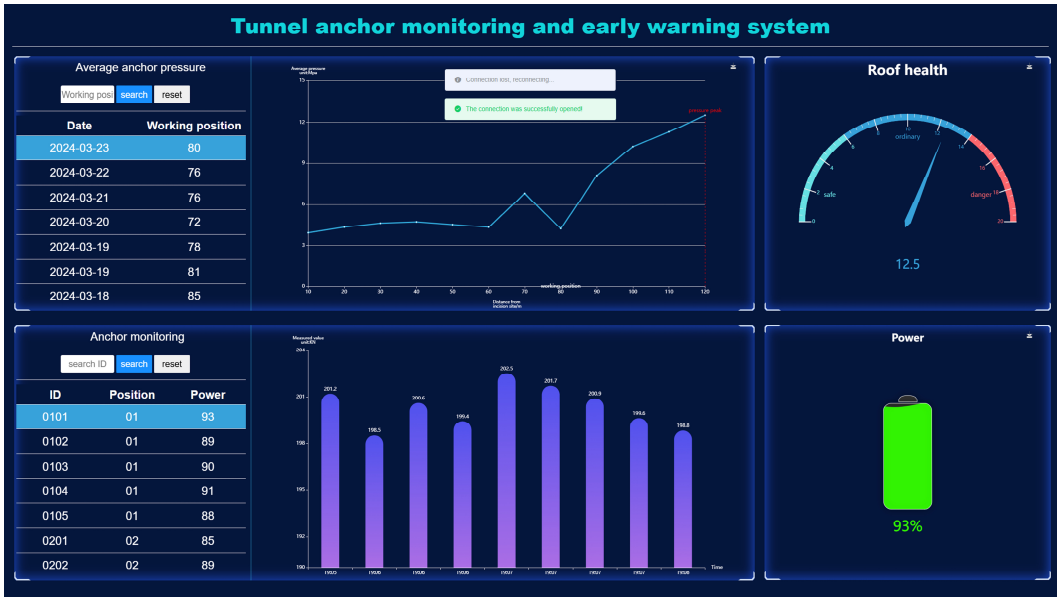

Figure 16. System reliability test.

In addition, the stability and performance of the system in processing large amounts of data were evaluated through the high-frequency data collection and transmission of nearly 400 sets of sensors in the actual project. As shown in Figure 17, this is the log of data received in the actual system project. It can be seen that the system can continuously receive 2–3 sets of data per second, which means the system can effectively handle high-frequency data reception, maintain stable operation, and provide accurate monitoring results. This proves that the system can still maintain reliability under high load conditions and has good processing capabilities.

```
topic:pSiXin data:1504,1735,635.0,91 time:  2024-03-25 15:45:50
topic:pSiXin data:3403,1726,289.5,91 time:  2024-03-25 15:46:00
topic:pSiXin data:203,1638,977.8,92 time:  2024-03-25 15:46:30
topic:pSiXin data:4,3784,4398.8,99 time:  2024-03-25 15:48:27
topic:pSiXin data:2401,1591,118.7,91 time:  2024-03-25 15:48:38
topic:pSiXin data:805,1702,0.0,79 time:  2024-03-25 15:49:02
topic:pSiXin data:804,1774,0.0,86 time:  2024-03-25 15:49:47
topic:pSiXin data:1805,1538,3.6,89 time:  2024-03-25 15:49:50
topic:pSiXin data:3304,1671,320.7,90 time:  2024-03-25 15:51:40
topic:pSiXin data:502,1670,158.1,89 time:  2024-03-25 15:51:41
topic:pSiXin data:803,1634,815.2,92 time:  2024-03-25 15:52:03
topic:pSiXin data:3501,1629,0.0,89 time:  2024-03-25 15:52:49
topic:pSiXin data:1205,1690,0.0,89 time:  2024-03-25 15:53:46
topic:pSiXin data:704,1689,239,4,91 time:  2024-03-25 15:54:37
topic:pSiXin data:604,1767,0.0,86 time:  2024-03-25 15:55:19
topic:pSiXin data:702,1785,3908.6,103 time:  2024-03-25 15:56:40
topic:pSiXin data:202,1707,7.7,89 time:  2024-03-25 15:57:36
topic:pSiXin data:201,1721,16.5,89 time:  2024-03-25 15:57:47
topic:pSiXin data:3704,1684,0.0,89 time:  2024-03-25 16:00:49
topic:pSiXin data:1401,1849,74.2,92 time:  2024-03-25 16:01:02
```

Figure 17. System receives pressure information log.

5.3. Prediction Model Validation

The LSTM–ARIMA-based tunnel anchor pressure prediction experiment was implemented on the dataset of anchor pressure in the transport tunnel of the Hulusu Coal Mine. There are 23,124 data records in the selected dataset, and the data collector sends pressure data every 30 min.

For the ARIMA model, the autocorrelation and partial autocorrelation plots of the training set are first drawn, as shown in Figure 18a,b. According to the Autocorrelation Coefficient (ACF) image, it is observed that the ACF decays rapidly and is obviously truncated when the lag order is 1, the time series has basically stabilized, and the difference part (d) can be set to 0. According to the PACF image, it is observed that the order (p) of the autoregressive part is tailed when the lag order is 1 or 2. This shows that the order (p) of the autoregressive part is 1 or 2. Finally, the ARIMA (1,0,1) model is selected as the ARIMA prediction model after analysis and comparison combined with the AIC.

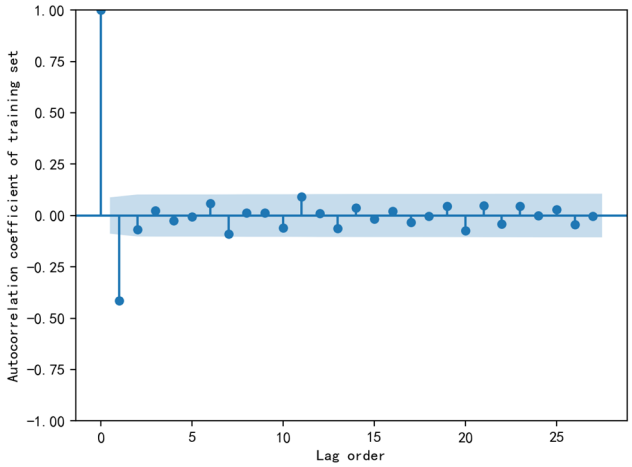

(**a**) Autocorrelation coefficient of training set

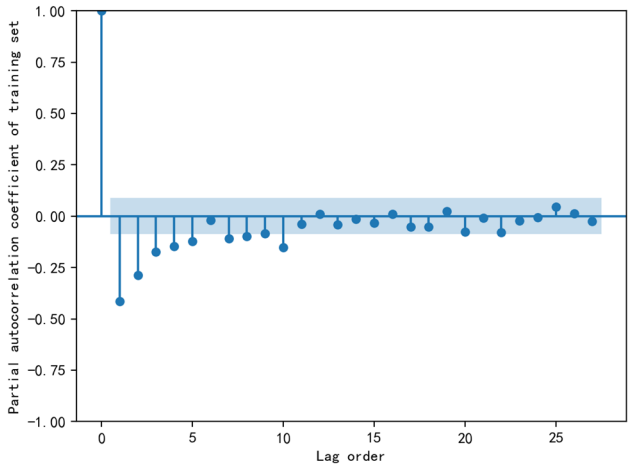

(**b**) Partial autocorrelation coefficient of training set

Figure 18. Training set autocorrelation coefficient and partial autocorrelation coefficient.

Based on the extracted anchor pressure data, the anchor pressure prediction model is obtained after data training, and then the test set is predicted. The errors of the two models and their weights during the prediction process are shown in Table 2. The prediction results are shown in Figure 19, where the horizontal axis represents the number of times every 30 min. Figure 19a shows the prediction result of the RNN model; Figure 19b shows the prediction result of the LSTM model; Figure 19c shows the prediction result of the ARIMA model; Figure 19d shows the prediction result of the LSTM–ARIMA combination model without dynamic weighting; and its weight is the fixed weight calculated for the first 100 times. Figure 19e shows the dynamic weighted prediction result of the LSTM–ARIMA combination model, and Figure 19f shows the error comparisons of the RNN, LSTM, ARIMA, and LSTM–ARIMA combination models without dynamic weighting and dynamic weighting prediction.

Table 2. Two model errors and their weights.

Number of Predictions	1	2	3	4	5	6	7	8	9	10
LSTM RMSE	0.823	0.817	0.817	0.821	0.820	0.809	0.822	0.821	0.820	0.814
ARIMA RMSE	0.844	0.839	0.839	0.844	0.843	0.831	0.840	0.838	0.835	0.826
LSTM Weights	0.506	0.507	0.507	0.507	0.507	0.507	0.505	0.505	0.505	0.504
ARIMA Weights	0.494	0.493	0.493	0.493	0.493	0.493	0.495	0.495	0.495	0.496

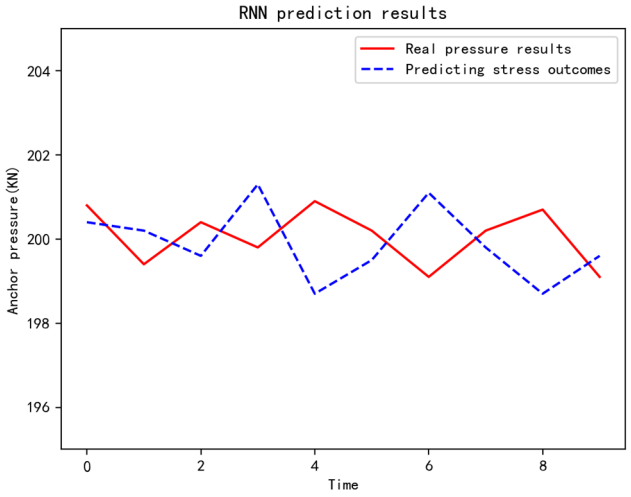

(**a**) RNN model prediction results

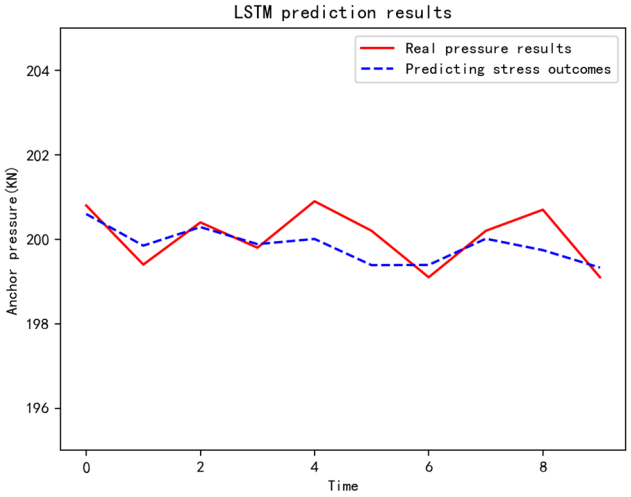

(**b**) LSTM model prediction results

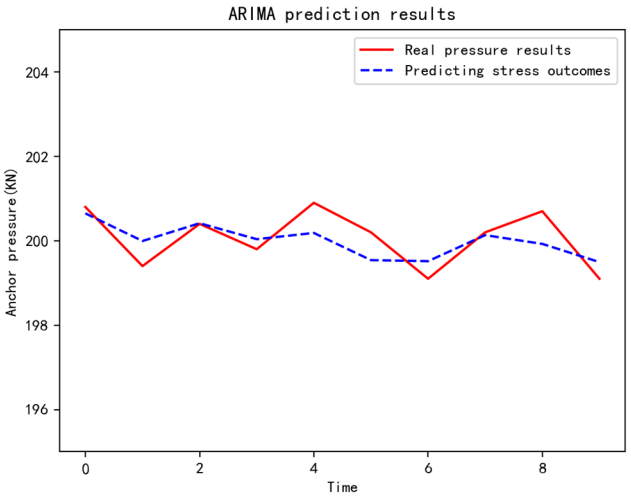

(**c**) ARIMA prediction results

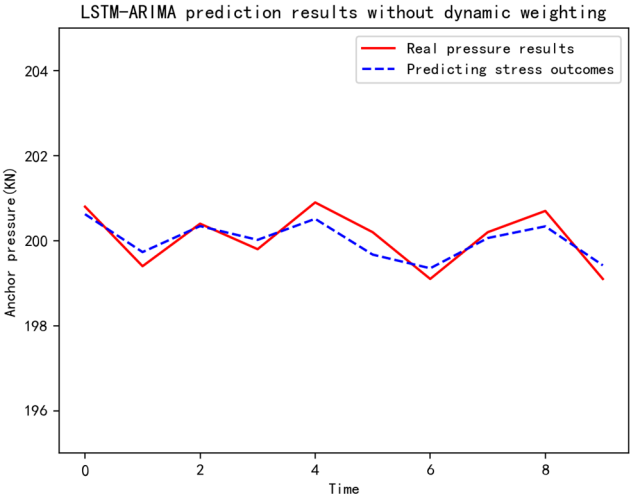

(**d**) LSTM–ARIMA prediction results without dynamic weighting model

Figure 19. *Cont.*

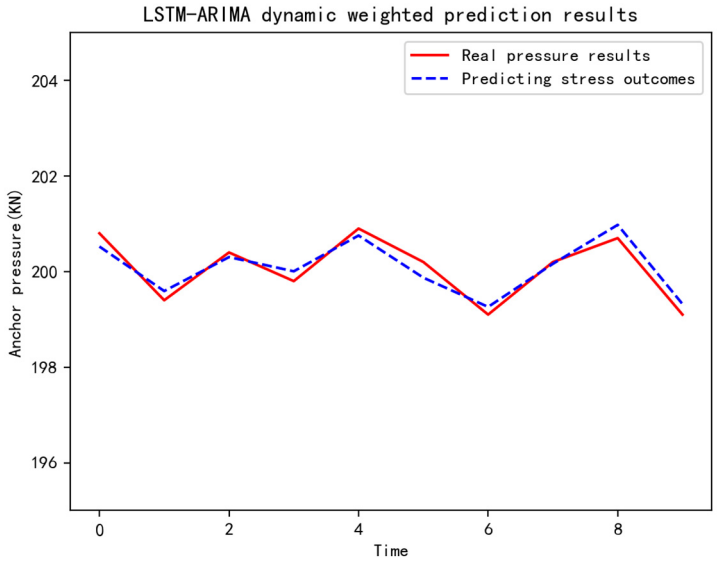

(**e**) LSTM–ARIMA dynamic weighted model prediction results

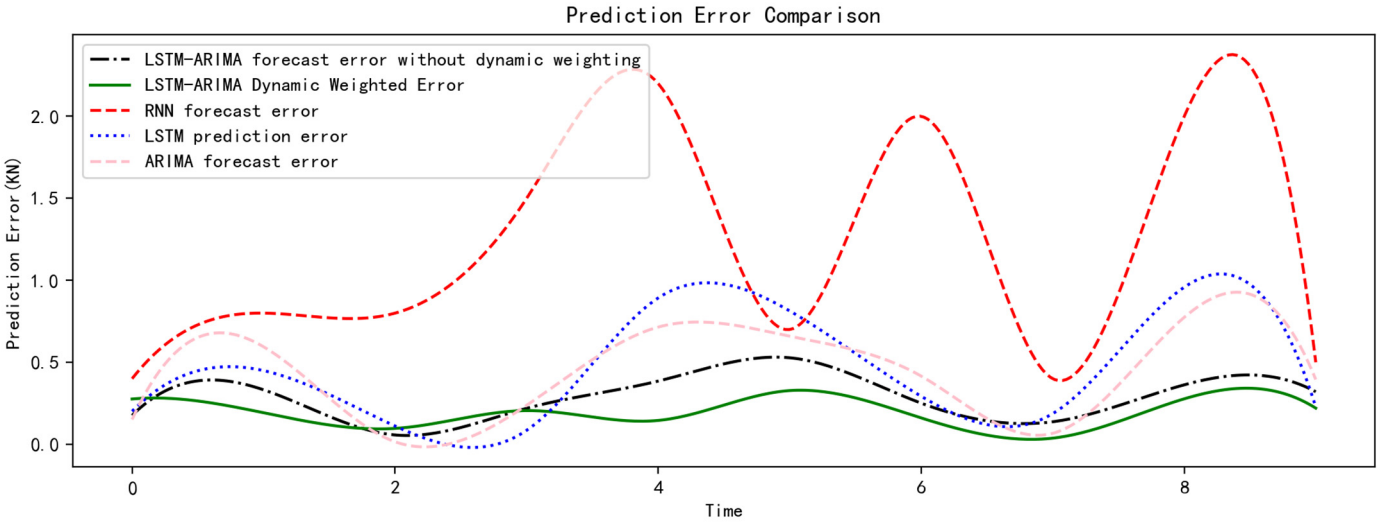

(**f**) Comparisons of prediction errors of five models

Figure 19. Comparisons of prediction results and errors of five models.

The error comparisons of the five models as the number of predictions increases are shown in Table 3.

Table 3. Comparisons of prediction errors among four models.

Number of Predictions	1	2	3	4	5	6	7	8	9	10
LSTM–ARIMA dynamic weighting prediction error (KN)	0.28	0.19	0.10	0.21	0.15	0.33	0.16	0.04	0.28	0.22
LSTM–ARIMA fixed weighting Forecast error (KN)	0.18	0.33	0.06	0.22	0.39	0.53	0.25	0.14	0.36	0.32
LSTM Prediction Error (KN)	0.20	0.45	0.11	0.09	0.89	0.81	0.29	0.19	0.96	0.23
ARIMA Prediction Error (KN)	0.15	0.59	0.02	0.24	0.71	0.66	0.42	0.07	0.77	0.40
RNN Prediction Error (KN)	0.42	0.83	0.82	1.56	2.24	0.71	2.02	0.44	2.06	0.56

The error results in Table 3 show that the average error of the single RNN model is 1.17 KN, and its maximum pressure error is 2.24 KN. The average error of the single

LSTM model is 0.42 KN, and its maximum pressure error is 0.96 KN. The average error of the single ARIMA model is 0.41 KN, and its maximum pressure error is 0.77 KN. The average error of the LSTM–ARIMA fixed weighted combination algorithm is 0.28 KN, and its maximum pressure error is 0.53 KN. The average error of the LSTM–ARIMA dynamic weighted combination algorithm is 0.20 KN, and its maximum pressure error is 0.33 KN. The LSTM–ARIMA dynamic weighted combination algorithm has the smallest error and a relatively gentle trend, which further shows that the prediction accuracy of the algorithm is better than that of the other four methods. The error of the LSTM–ARIMA dynamic weighted combination algorithm is controlled within 0.5 KN. In actual projects, the anchor pressure is within the normal range of 140–400 KN. At the same time, due to the complex environment of underground tunnels, the pressure value measured using the sensor may fluctuate due to environmental conditions, equipment accuracy, and other factors. In actual measurements, the pressure value fluctuates by 1 KN, which is within the normal range. Therefore, an error of 0.5 KN meets the anchor pressure prediction requirements and verifies the effectiveness of the proposed model in the prediction of anchor support forces in coal mine tunnels.

6. Conclusions

Aimed at the current problems with the stability monitoring of the anchor support system in underground coal mine tunnels, a tunnel anchor monitoring system is constructed, and an LSTM–ARIMA dynamic weighted prediction model is established based on confidence, achieving the real-time monitoring and prediction of anchor pressure.

(1) The LSTM–ARIMA dynamic weighted combination model based on confidence can capture the dynamic patterns and changing trends in the time series data and improve the accuracy of prediction results compared with the single model and the LSTM–ARIMA fixed weighted combination model.

(2) The prediction results of anchor pressure in the tunnel show that the average error of anchor pressure prediction is 0.20 KN, and all anchor pressure prediction errors are less than 0.5 KN during the whole prediction process, which effectively meets the needs of tunnel monitoring and verifies the effectiveness of the proposed LSTM–ARIMA method.

(3) The reliability and robustness of the system are proven by testing on datasets obtained from actual projects. The system can respond and handle various abnormal situations in a timely manner and maintain stable operation and accurate monitoring results, which provides a reliable guarantee for the practical application of the system in coal mine tunnel bolt support monitoring and ensures the reliability and accuracy of the monitoring data.

Author Contributions: Conceptualization, Y.C. and J.Q.; methodology, Y.C.; program, Y.C.; validation, Y.C., J.Q. and L.W.; formal analysis, Y.C.; investigation, Y.C.; resources, Y.C.; data curation, Y.C.; writing—original draft preparation, Y.C.; writing—review and editing, Y.C., J.Q. and L.W.; visualization, Y.C.; supervision, J.Q. and L.W.; project administration, R.Y.; funding acquisition, J.Q. All authors have read and agreed to the published version of the manuscript.

Funding: This work is supported by the Program for Innovative Research Team (in Science and Technology) at the University of Henan Province (22IRTSTHN005) and the "Double first class" discipline creation project of Henan Polytechnic University (AQ202300403).

Data Availability Statement: Datasets cannot be made public for copyright reasons.

Conflicts of Interest: The authors declare no conflicts of interest.

References

1. Cheng, C.; Gao, D.; Zhang, H.; Xu, Z.; Huang, J. Superstructure optimization models for regional coal industry development considering water resources constraints—A case study of Ordos, China. *Comput. Chem. Eng.* **2023**, *178*, 108384. [CrossRef]
2. Wang, F.; Jiang, B.; Chen, S.; Ren, M. Surface collapse control under thick unconsolidated layers by backfilling strip mining in coal mines. *Int. J. Rock Mech. Min. Sci.* **2019**, *113*, 268–277. [CrossRef]

3. Yao, J.; Han, K.; Zhu, W.; Cao, Y. Research on Collapse Detection in Old Coal Mine Goafs Based on Space–Sky–Earth Remote Sensing Survey. *Remote Sens.* **2024**, *16*, 1164. [CrossRef]
4. Liu, T.; Xu, D.; Shi, L.; Qu, L.; Ji, K. Trapezoidal collapse model to calculate the height of the overburden collapse zone in coal seam mining: An example from Guo'Jiahe Coal Mine, Western China. *Energy* **2022**, *256*, 124609. [CrossRef]
5. Wang, L.; Sun, K.; Qi, J.; Yuan, R. Distributed High-Density Anchor (Cable) Support Force Monitoring System Research. *Electronics* **2024**, *13*, 2221. [CrossRef]
6. Liu, S.; He, D.; Fu, M. Experimental investigation of surrounding-rock anchoring synergistic component for bolt support in tunnels. *Tunn. Undergr. Space Technol.* **2020**, *104*, 103531. [CrossRef]
7. Wang, W.; Pan, Y.; Xiao, Y. Synergistic resin anchoring technology of rebar bolts in coal mine roadways. *Int. J. Rock Mech. Min. Sci.* **2022**, *151*, 105034. [CrossRef]
8. Yuan, H.; Li, Y.; Zhou, B.; He, S.; Wang, P. Friction Characteristics of Post-Tensioned Tendons of Full-Scale Structures Based on Site Tests. *Adv. Civ. Eng.* **2020**, *2020*, 5916738. [CrossRef]
9. Fu, J.; Guo, Y.; Li, P. A Fiber Bragg Grating Anchor Rod Force Sensor for Accurate Anchoring Force Measuring. *IEEE Access* **2020**, *8*, 12796–12801. [CrossRef]
10. Kou, H.-L.; Li, W.; Zhang, W.-C.; Zhou, Y.; Zhou, X.-L. Stress Monitoring on GFRP Anchors Based on Fiber Bragg Grating Sensors. *Sensors* **2019**, *19*, 1507. [CrossRef]
11. Miao, Q.; Huang, B. On the optimal anchor placement in single-hop sensor localization. *Wirel. Netw.* **2018**, *24*, 1609–1620. [CrossRef]
12. Kou, H.; Guo, W.; Zhang, M. Pullout performance of GFRP anti-floating anchor in weathered soil. *Tunn. Undergr. Space Technol.* **2015**, *49*, 408–416. [CrossRef]
13. Liu, J. Enhanced prediction of bolt support drilling pressure using optimized Gaussian process regression. *Sci. Rep.* **2024**, *14*, 2247. [CrossRef]
14. Gao, X.; Tian, W.; Li, J.; Qi, H.; Zhang, Z. Research on Prediction Model of Prestress Loss of Anchor Cable in Soil-Rock Dual-Structure Slope. *Adv. Mater. Sci. Eng.* **2021**, *2021*, 1–10. [CrossRef]
15. Ostmeyer, J.; Cowell, L. Machine learning on sequential data using a recurrent weighted average. *Neurocomputing* **2019**, *331*, 281–288. [CrossRef] [PubMed]
16. Hochreiter, S.; Schmidhuber, J. Long Short-Term Memory. *Neural Comput.* **1997**, *9*, 1735–1780. [CrossRef] [PubMed]
17. Soto, J.; Castillo, O.; Melin, P.; Pedrycz, W. A New Approach to Multiple Time Series Prediction Using MIMO Fuzzy Aggregation Models with Modular Neural Networks. *Int. J. Fuzzy Syst.* **2019**, *21*, 1629–1648. [CrossRef]
18. Eskandari, H.; Imani, M.; Moghaddam, M.P. Convolutional and recurrent neural network based model for short-term load forecasting. *Electr. Power Syst. Res.* **2021**, *195*, 107173. [CrossRef]
19. Li, Y.; Wu, K.; Liu, J. Self-paced ARIMA for robust time series prediction. *Knowl.-Based Syst.* **2023**, *269*, 110489. [CrossRef]
20. Diaz, J.; Agioutantis, Z.; Hristopulos, D.T.; Luxbacher, K.; Schafrik, S. Forecasting of methane gas in underground coal mines: Univariate versus multivariate time series modeling. *Stoch. Environ. Res. Risk Assess.* **2023**, *37*, 2099–2115. [CrossRef]
21. Odaki, M. On the invertibility of fractionally differenced ARIMA processes. *Biometrika* **1993**, *80*, 703–709. [CrossRef]
22. Solo, V. The Order of Differencing in ARIMA Models. *J. Am. Stat. Assoc.* **1984**, *79*, 916–921. [CrossRef]
23. Siddique, M.A.B.; Mahalder, B.; Haque, M.M.; Shohan, M.H.; Biswas, J.C.; Akhtar, S.; Ahammad, A.K.S. Forecasting of tilapia (*Oreochromis niloticus*) production in Bangladesh using ARIMA model. *Heliyon* **2024**, *10*, e27111. [CrossRef]